Effects of A-site atoms in Ti2AlC and Ti3SiC2 MAX phases reinforced Mg composites: Interfacial structure and mechanical properties

Wenbo Yu, Xufeng Pi, Wantong Chen, Maxime Vallet, Antoine Guitton, Laiqi Zhang

Effects of A-site atoms in Ti_2AlC and Ti_3SiC_2 MAX phases reinforced Mg composites: Interfacial structure and mechanical properties

Wenbo Yu [a,*], Xufeng Pi [a], Wantong Chen [a], Maxime Vallet [b], Antoine Guitton [c], Laiqi Zhang [d]

[a] Center of Materials Science and Engineering, School of Mechanical and Electronic Control Engineering, Beijing Jiaotong University, Beijing, 100044, China
[b] Laboratoires MSSMat (UMR 8579) et SPMS (UMR 8580), CentraleSupélec, Université Paris-Saclay, 91190, Gif-sur-Yvette, France
[c] Université de Lorraine, CNRS, Arts et Métiers, LEM3 and Labex Damas, Université de Lorraine, France
[d] State Key Laboratory for Advanced Metals and Materials, University of Science and Technology Beijing, 100083, China

ARTICLE INFO

Keywords:
Casting Ti_3SiC_2 MAX phase
Tensile fracture
Microstructural observation

ABSTRACT

AZ91D magnesium composites reinforced by Ti_3SiC_2 MAX phase were fabricated by the stir casting technique. Tensile tests reveal that the reinforced effects of Ti_3SiC_2 and Ti_2AlC on Mg matrix are different. Unlike Ti_2AlC-AZ91D composite for which Ti_2AlC delamination happens during the fracture, Ti_3SiC_2-AZ91D composite fractures by interfacial debonding mechanisms. Transmission electron microscopy characterization shows that few nanometric Mg grains form in the vicinity of Ti_3SiC_2 particles, while huge amount of nanometric Mg grains form along with Ti_2AlC particles. Elements mapping confirms that Al atoms of Ti_2AlC diffuse into Mg matrix. In contrast, no outward diffusion of Si of Ti_3SiC_2 is observed. This outcome points out that it is possible to regulate the mechanical properties of their relevant Mg composite through adjusting the content of Al and Si in MAX phases, such as Ti_3SiAlC_2 solid solution.

1. Introduction

Magnesium alloy is regarded as one of the most promising structural materials candidates in the aerospace and automobile industry, especially in applications subjected to strong acceleration and high speed [1,2], due to its lightweight, high specific strength and high damping capacity [3,4]. It is reported that light-weighting offers up to a 7% improvement in fuel economy for each 10% reduction in vehicle weight [5]. However, the poor elevated temperature tensile strength of Mg-based materials restricts their wide utilization for applications [6,7], especially in the area, where high stiffness, high wear resistance and damping capacity are strongly desired. The only way for optimizing these properties is to introduce reinforcement into Mg alloy.

Recently, ternary and nano-layered compounds, named as MAX phases ($M_{n+1}AX_n$, where M is early transition metal, A belongs to group IIIA or IVA element, X is C and/or N, N = 1–3) [8,9], were introduced into Mg alloy due to their unique combination of metal-like and ceramic-like properties [10–12]. In comparison with traditional binary ceramic particles (e.g. TiC and SiC) [13–15], Barsoum et al. [8] found that MAX phases could dissipate energy capacity due to its kinking nonlinear elastic (KNE) mechanism. Anasori et al. reported that Mg composites reinforced with 20 vol% Ti_2AlC could dissipate 30% mechanical energy during each compressive load at 250 MPa [16]. Yu et al. [17–20] systematically investigated Ti_2AlC-AZ91D magnesium composite fabricated by semi-solid stirring method and processed with hot extrusion. Unlike SiC-AZ91D composite for which interfacial decohesion is found after tensile test, the *in-situ* tensile tests have revealed that micro-cracks are initiated from the Ti_2AlC basal planes rather than from the Ti_2AlC–Mg interface. The high damping capacity of Ti_2AlC-AZ91D magnesium composite comes from the high dislocation density contained in Ti_2AlC and Mg matrix at room temperature. Furthermore, Ti_2AlC-AZ91D magnesium composite simultaneously exhibits high wear resistance and self-lubricated capacity. Unlike hard ceramic particles, such as SiC, no severe grooves and scratches were found on the magnesium matrix surface due to the easy pulling out of hard ceramic particles [13]. Even though the introduction of lubricant graphene, graphite and MoS_2 could decrease the coefficient of friction, such as B_4C-Graphite/Mg [14] and SiC-Graphene/Mg [15], graphite and MoS_2 degrade rapidly at above 350 °C in an oxidizing environment.

MAX phases contain more than 70 different species and A elements are easily out-diffused from MAX unit cell. For example, migration energy of Si in Ti_3SiC_2 (0.9 eV) [21,22] is higher than that of Al in Ti_2AlC (0.83 eV). This means that it is possible to regulate the interfacial structure of MAX-Mg by replacing Ti_2AlC with Ti_3SiC_2. As reported in

* Corresponding author.
E-mail address: wbyu@bjtu.edu.cn (W. Yu).

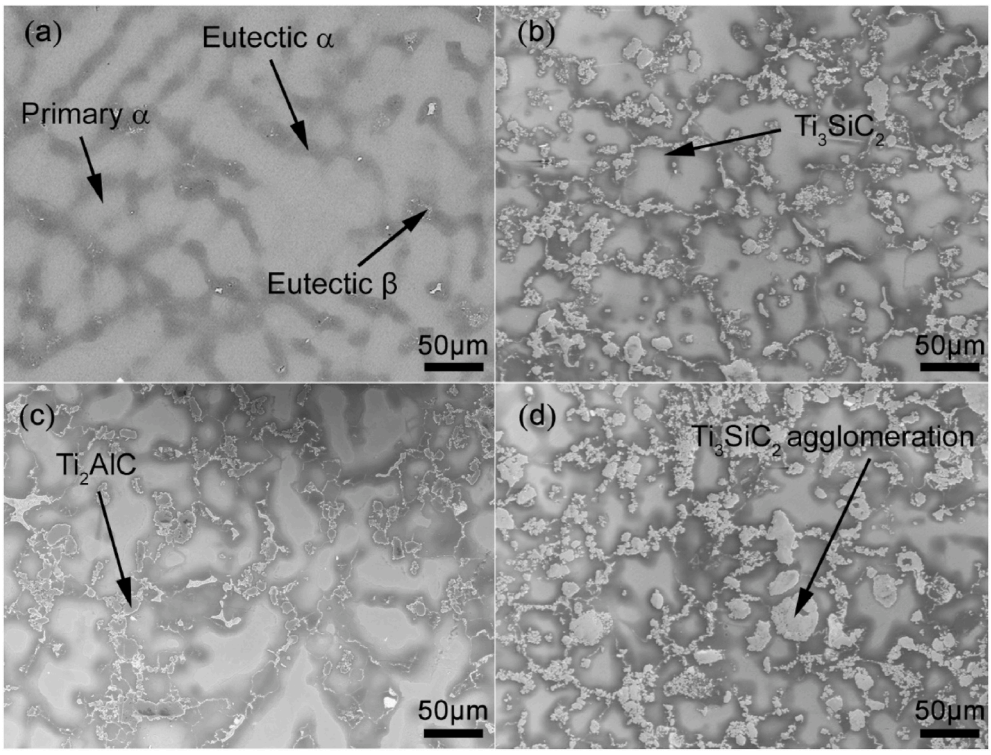

Fig. 1. Backscattered electron (BSE) micrographs of (a) as-cast AZ91D alloy and the composites reinforced with (b) 5 vol% Ti_3SiC_2, (c) 5 vol% Ti_2AlC and (d) 15 vol % Ti_3SiC_2.

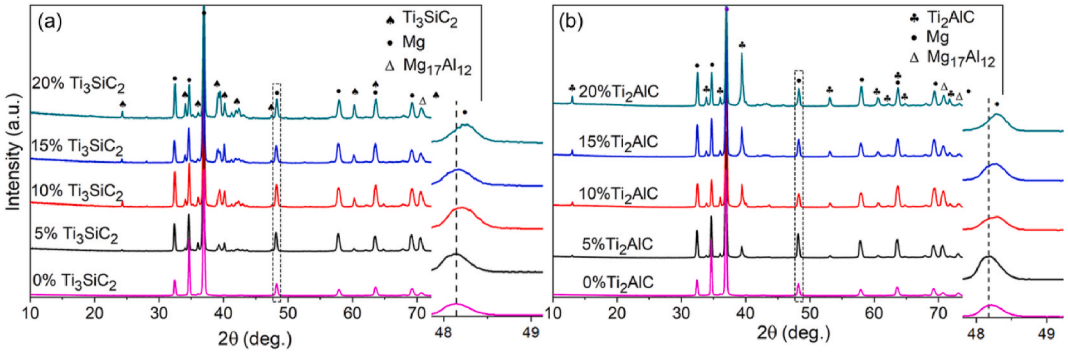

Fig. 2. XRD diffractograms of as-cast (a) Ti_3SiC_2-AZ91D and (b) Ti_2AlC-AZ91D [24] composites.

our previous study [19], the interfacial friction could not be activated until 200 °C. In addition, Al_2O_3 and MgO were detected on the surface of Ti_2AlC-AZ91D magnesium composite during the dry-slide test, which is detrimental to the tribological properties. Furthermore, the formed nano Mg grains did not coarsen in Ti_2AlC–Mg composite under heating 3 times to 700 °C, while this phenomenon is not found in Ti_3SiC_2–Mg composite [23]. Herein, in order to clarify this phenomenon and characterize their reinforcement capacity in magnesium composite, we fabricated two composites Ti_2AlC-AZ91D and Ti_3SiC_2-AZ91D. Then we compared their mechanical properties and investigate their interfacial evolution.

2. Experimental method

In this work, AZ91D magnesium alloy (Al: 9.0, Zn: 0.81, Si: 0.1, Mn: 0.24, Fe: 0.022, Cu: 0.030, Ni: 0.005, Mg: rest) reinforced by laboratory-made Ti_3SiC_2 particles (diameter below 10 μm) was fabricated by semi-solid stirring method. The Ti_3SiC_2 powders were synthesized from starting powders of Titanium (Ti, 99.5% purity), silicon (Si, 99.5% purity) and titanium carbide (TiC, 99.5% purity) powders with a molar ratio of 3Ti: 1.1Si: 1.9C by pressureless sintering at 1500 °C during 20 min under Ar gas protection. The AZ91D alloy ingots were heated to be 700 °C under the protection of CO_2/SF_6 gas and cooled to the semi-solid condition (590 °C). Then, the preheated Ti_3SiC_2 particles were poured into the high speed stirred (1000 rpm) semi-solids. After homogeneous stirring, the melt was reheated to be 700 °C and poured into a preheated metal mold (450 °C). Finally, the 100 MPa was applied on a servo press machine during solidification. More details can be found in our previous study about Ti_2AlC-AZ91D composite [24].

Uniaxial tensile tests were performed through a universal servo-hydraulic mechanical testing machine (Instron 5600, Norwood, MA) with a strain rate of 0.5 mm/min at room temperature. The specimens were prepared with the dimension of 18 mm long (gauge), 3 mm wide and 2 mm thick in reference to the ASTM E8M – 03 flat specimen standard.

Phase identification was performed by X-Ray Diffraction (XRD) using a Bruker (Karlsruhe, Germany) D8 diffractometer with CuK_a radiation. Microstructural observation was carried out by Scanning Electron

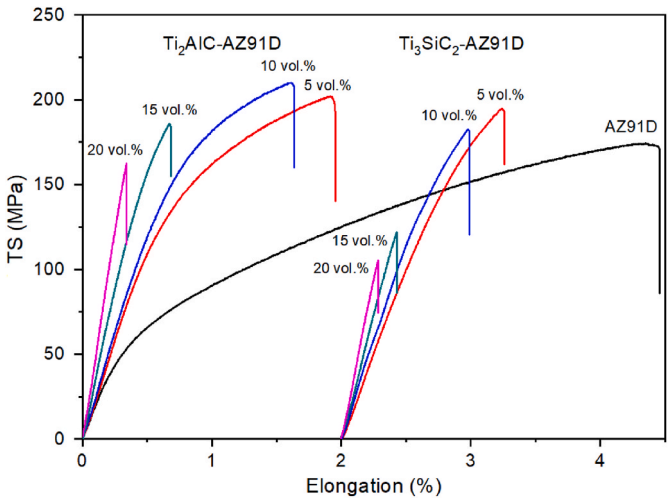

Fig. 3. The room temperature tensile stress-strain curves of the as-cast AZ91D and its composites reinforced by Ti_2AlC and Ti_3SiC_2.

Table 1
Mechanical properties of the as-cast AZ91D alloy and its composites reinforced by Ti_2AlC and Ti_3SiC_2, including Elasticity moduli (E), 0.2% yield strengths (YS), ultimate tensile strengths (UTS).

Materials	E (GPa)	YS (MPa)	UTS (MPa)	Ref.
AZ91D	40 ± 1	70 ± 2	175 ± 5	this work
5 vol% Ti_3SiC_2-AZ91D	46 ± 1	178 ± 3	195 ± 6	this work
10 vol% Ti_3SiC_2-AZ91D	55 ± 1	173 ± 3	180 ± 6	this work
15 vol% Ti_3SiC_2-AZ91D	66 ± 2	–	120 ± 4	this work
20 vol% Ti_3SiC_2-AZ91D	76 ± 2	–	105 ± 4	this work
5 vol%Ti_2AlC-AZ91D	52	108	200	[24]
10 vol% Ti_2AlC-AZ91D	56	135	215	[24]
15 vol%Ti_2AlC-AZ91D	62	145	185	[24]
20 vol%Ti_2AlC-AZ91D	69	160	165	[24]

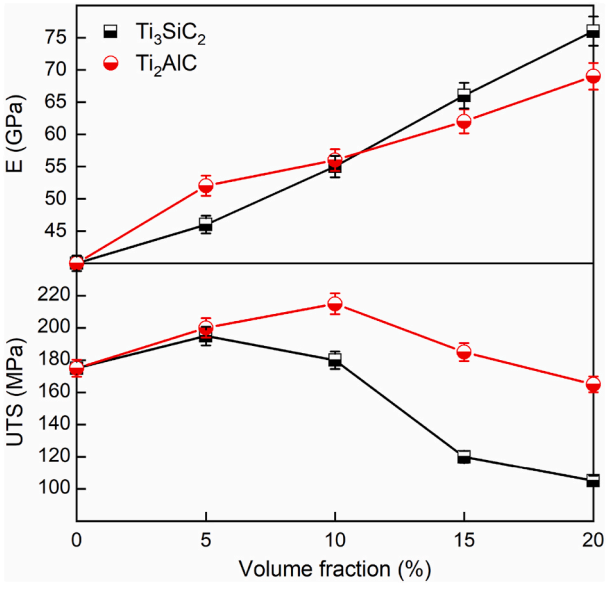

Fig. 4. Elasticity moduli (E) and ultimate tensile strengths (UTS) of Ti_3SiC_2-AZ91D and (b) Ti_2AlC-AZ91D composites as a function of the reinforcement volume fraction.

Microscopy (ZEISS, Germany). For interfacial observation, the cross-sectional slices were cut with FIB in a dual-beam FIB/SEM (Carl Zeiss AURIGA Cross Beam Workstation, Germany) with Ga ion source at 30 kV. Scanning Transmission Electron Microscopy (STEM) coupled with Energy Dispersive X-ray spectroscopy (EDX) chemical analyses were carried out in a CM20-FEG working at 200 kV equipped with a Micro-analyser QUANTAX XFlash detector.

3. Results

Fig. 1 shows the microstructure of the as-cast AZ91D alloy and composites reinforced with different MAX phases. As found in Fig. 1a-c, no matter the introduction of Ti_3SiC_2 or Ti_2AlC, the composites present the similar microstructure. MAX phases particles distribute along grain boundaries of the primary α-Mg phase and coexist with eutectic α (Mg) and β ($Mg_{17}Al_{12}$) phases. As previously observed on Ti_2AlC-AZ91D composite [24], when the introduction of Ti_3SiC_2 particles increased from 5 vol% to 15 vol%, the agglomeration of Ti_3SiC_2 particles appeared (Fig. 1d).

Fig. 2 shows the XRD diffractograms of Ti_3SiC_2-AZ91D and Ti_2AlC-AZ91D composites. No impurities are detected in both two composites. The shift of Mg peak appeared for all of Mg peaks. For example, it is clear that the Mg peak (103) at around 2θ of 48° continuously shifts with the increasing content of Ti_2AlC particles in Ti_2AlC-AZ91D composite, while it is much less clear in Ti_3SiC_2-AZ91D composite. During the solidification, as most particles are segregated in the intergranular regions during the impingement with other growing grains [25,26], the growth of dendritic α-Mg is restricted and produces a compressive force. The difference in these two composites suggests that much higher compressive force formed around Mg grains with the increasing Ti_2AlC volume in Ti_2AlC-AZ91D composite.

Fig. 3 plots the room temperature tensile stress-strain curves of as-cast AZ91D and its composites reinforced by Ti_2AlC and Ti_3SiC_2. With the introduction of more MAX particles, the ductility of composites strongly decreased, especially for Ti_3SiC_2-AZ91D composite. The composites reinforced with 15 vol% and 20 vol% Ti_3SiC_2 particles did not even reach the summit of yield strength before fracture. Table 1 summarizes the elastic moduli (E), tensile yield strength, and ultimate tensile strength (UTS) values of the different specimens. For clarity, E and UTS values of the two composites are plotted as a function of reinforcement volume fraction (Fig. 4). E of both composites are continuously enhanced with the increasing content of reinforcement, especially for the case of Ti_3SiC_2. Such a result is supposed to be the difference in E between Ti_2AlC (277 GPa) [27] and Ti_3SiC_2 (343 GPa) [28]. Regarding UTS, the UTS of AZ91D alloy is enhanced when 5 vol% of Ti_2AlC or Ti_3SiC_2 MAX phase is introduced into magnesium alloy. Similar to the results found in Ti_2AlC-AZ91D composite [24], the addition of Ti_3SiC_2 could refine the grains of α-Mg and produce the Hall-Petch effect. After, the UTS of Ti_2AlC-AZ91D composites increases with the introduction of Ti_2AlC from 5 vol% to 10 vol%, then decreases with more introduction of Ti_2AlC. Differently, UTS of Ti_3SiC_2-AZ91D continuously decreases with the increasing content of Ti_3SiC_2 volume fraction. In addition, the UTS Ti_2AlC-AZ91D composite is higher than that of Ti_3SiC_2-AZ91D for each volume fraction. This phenomenon was also reported by Anasori et al. [29] who studied the MAX phases particles (50 vol%) reinforced Mg composites fabricated by pressureless melt infiltration method. In order to clarify this difference, the tensile fracture surface and interfacial evolution in these two composites were further exploited in the following part.

4. Discussion

Fig. 5a and b shows the tensile fracture morphologies of AZ91D composites reinforced by 5 vol% and 15 vol% Ti_3SiC_2. Tear edges in Mg matrix are strongly reduced with the increasing content of Ti_3SiC_2 particles in composites. However, as found in Fig. 5b and c, Ti_3SiC_2 and

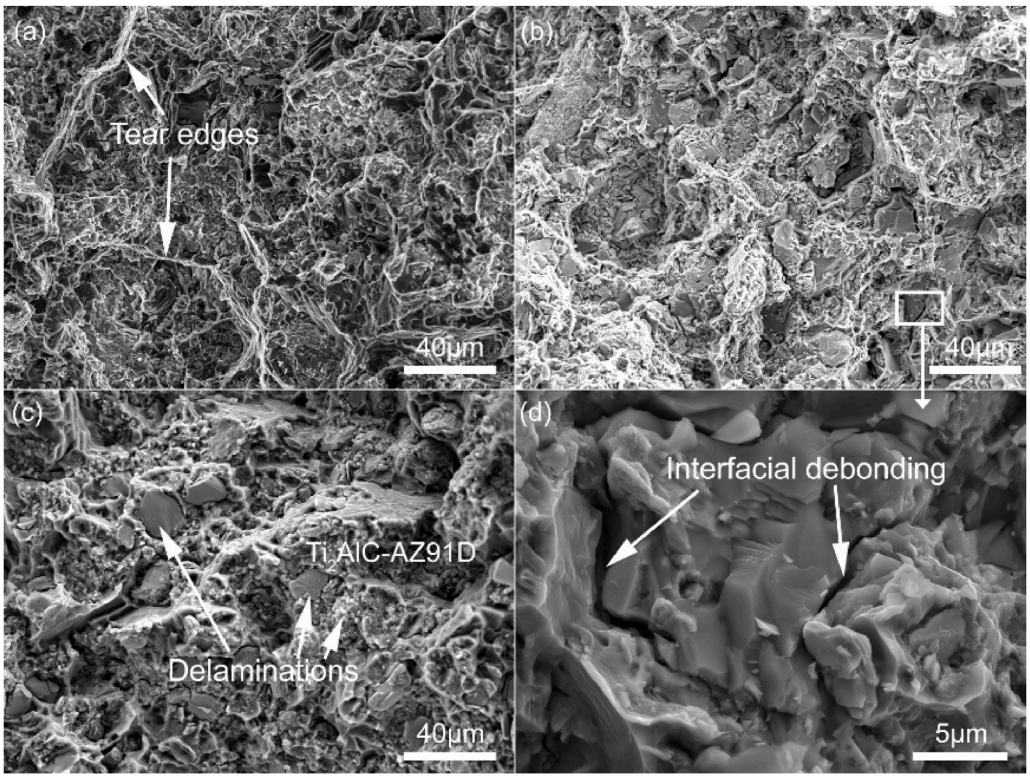

Fig. 5. Tensile fracture surfaces of the AZ91D composite reinforced with (a) 5 vol% Ti_3SiC_2, (b, d) 15 vol% Ti_3SiC_2 and (c) 15 vol% Ti_2AlC.

Ti_2AlC particles exhibit different fracture behavior in MAX particles. The enlarged area shown in Fig. 5d indicates that Ti_3SiC_2 particles are detached from Mg matrix due to the interfacial decohesion. However, no interfacial decohesion was observed in Ti_2AlC-AZ91D composite. In Fig. 5c, the clean and flat fracture surface of Ti_2AlC indicates that delamination occurred in Ti_2AlC particles.

Fig. 6 presents the high-angle annular dark field (HAADF) micrographs of Ti_3SiC_2-AZ91D and Ti_2AlC-AZ91D interfaces. As shown in Fig. 6a and b, no nanometric Mg grains were found in the vicinity of Ti_3SiC_2 particles. However, Fig. 6c and d reveal the formation of nanometric Mg grains among Ti_2AlC particles. This agrees with the results reported by Amini et al. [30]. In addition, different contrasts can be observed in Mg matrix among Ti_2AlC particles. Fig. 7 shows the magnified area marked in Fig. 6c. Closed to the interface, the nano Mg grains become smaller. The corresponding diffraction patterns of selected areas confirmed this phenomenon. The polycrystalline rings were found in region 2 and 3, especially in region 2. This indicates that a finer polycrystalline magnesium tends to form on the Ti_2AlC surface. As the formation of nano-sized Mg grains among Ti_2AlC particles could strongly strengthen the metal matrix due to the Hall-Petch effect [30–32], the UTS of Ti_2AlC-AZ91D composite is higher than that of Ti_3SiC_2-AZ91D for each volume fraction.

Fig. 8 shows the images taken close to the interfaces of the composites accompanied with the corresponding elemental EDX maps of Ti, Al and Si. Fig. 8b-c show that maps of Ti and Si exhibit identical distribution in Ti_3SiC_2-AZ91D composite. However, Fig. 8f-g indicate that the Al zone is much bigger than that of Ti in Ti_2AlC-AZ91D composite. The Al distribution in Fig. 8g suggests that Al atoms in Ti_2AlC outwards diffused into AZ91D magnesium matrix. Finally, nano Mg grains formed among Ti_2AlC particles. In addition, the out-diffusion of Al atoms may arouse the formation of a thin amorphous magnesium layer between Ti_2AlC and nano Mg grains. This robust amorphous layer was respectively found by Yu et al. [17] and Amini et al. [30]. Khoddam et al. pointed that the robust amorphous layer could reduce the interfacial energy of incoherent interface due to large lattice mismatch and therefore promote the interfacial bonding strength [33]. Herein, interfacial decohesion happens in Ti_3SiC_2-AZ91D composite, while not found in Ti_2AlC-AZ91D composite.

This difference is maybe aroused by different solubility between Al and Si in magnesium matrix or by the different migration energy between Al and Si in MAX phases. First-principles calculations show that the migration energy of Al in Ti_2AlC (0.83 eV) is lower than that of Si in Ti_3SiC_2 (0.9 eV) [21,22], which indicates that out-diffusion of Si from Ti_3SiC_2 is much harder than Al from Ti_2AlC under the same conditions. It has been experimentally proved that the ratio between Al and Si in $Ti_3(Si_{1-x}Al_x)C_2$ solid solution can be arbitrarily regulated [34]. This means that it could be possible to control the interface bonding strength between Ti_3SiC_2 and Mg Matrix with the formation of $Ti_3(Si_{1-x}Al_x)C_2$ solid solution.

5. Conclusion

Both Ti_3SiC_2 and Ti_2AlC (5, 10, 15, 20 vol%) reinforced AZ91D magnesium composites were fabricated under 700 °C by the stir casting method and compared. As previously observed on Ti_2AlC-AZ91D composite [24], an agglomeration of particles occurred when the

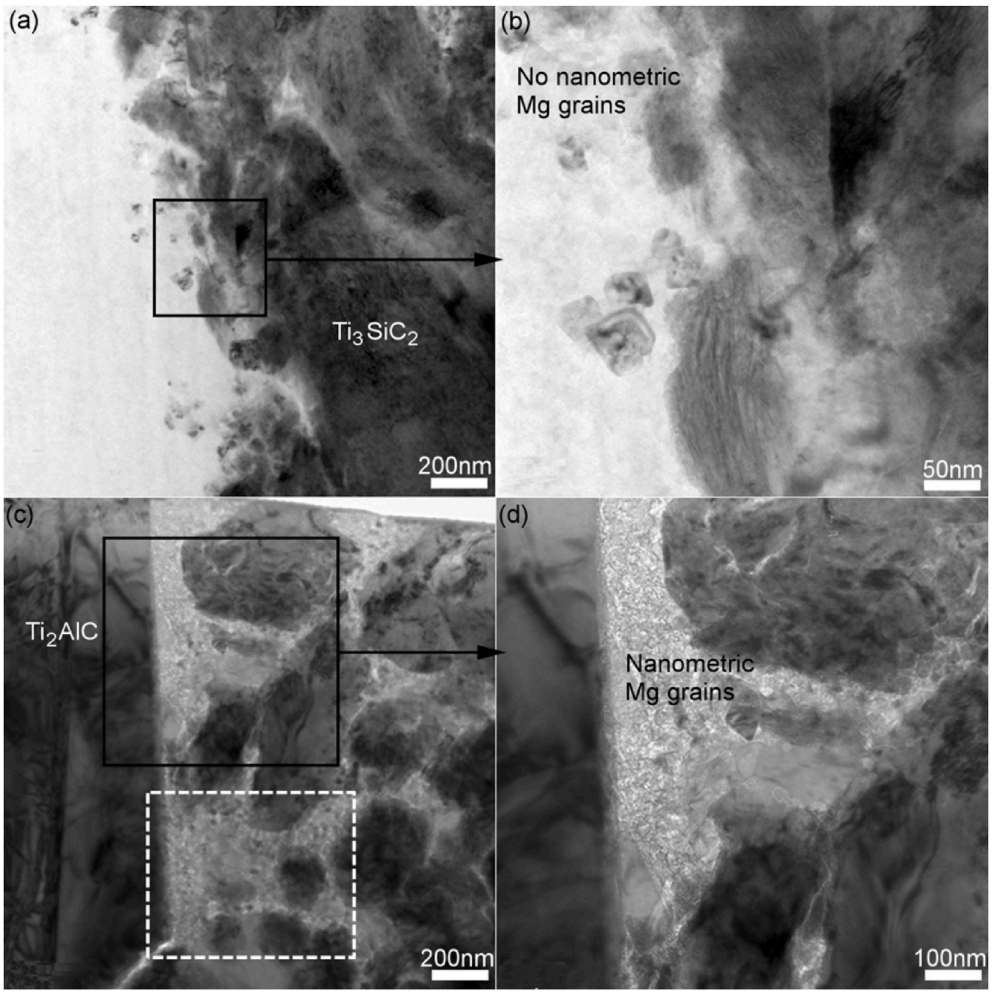

Fig. 6. HAADF micrographs of (a, b) Ti_3SiC_2-AZ91D and (c, d) Ti_2AlC-AZ91D interfaces.

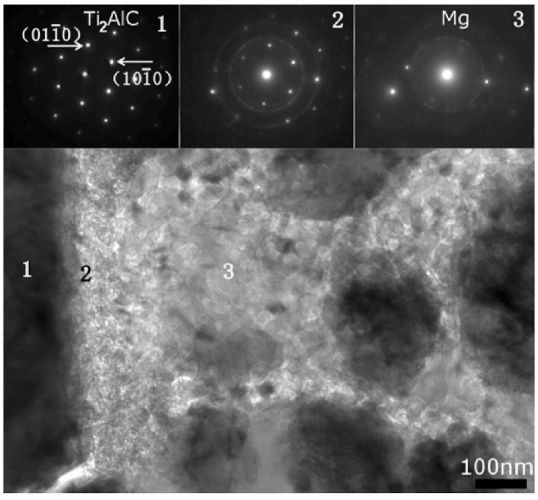

Fig. 7. Enlarged area marked with a dotted box in Fig. 6c and selected area electron diffraction patterns of the zones marked as 1, 2 and 3.

introduction of Ti_3SiC_2 particles is higher than 5 vol%. A slight and continuous shift of the Mg peaks appears with the increasing content of Ti_2AlC particles due to the formation of nanometric Mg grains, while this phenomenon was not found in the case of Ti_3SiC_2-AZ91D composite.

Ti_3SiC_2 particles were detached from Mg matrix due to the interfacial decohesion. However, no interfacial decohesion has been observed in Ti_2AlC-AZ91D composite. Herein, the UTS of Ti_3SiC_2-AZ91D composite is much lower than that of Ti_2AlC-AZ91D composite. TEM analyses have revealed that the outwards diffusion of Al from Ti_2AlC into Mg matrix aroused the formation of the thin amorphous magnesium and nano Mg grains among Ti_2AlC particles. In contrast, no outwards diffusion of Si from Ti_3SiC_2 into Mg matrix was detected. This study suggests that it is possible to control the interface bonding strength between Ti_3SiC_2 and Mg matrix through the ratio design between Al and Si in $Ti_3(Si_{1-x}Al_x)C_2$ solid solution.

CRediT authorship contribution statement

Wenbo Yu: Conceptualization, Methodology, Investigation, Writing. **Xufeng Pi:** Resourses. **Wantong Chen:** Resourses. **Maxime Vallet:** Language polish and revison. **Antoine Guitton:** Language polish and revison. **Laiqi Zhang:** Writing – review & editing.

Declaration of competing interest

The authors declare the following financial interests/personal relationships which may be considered as potential competing interests: The experimental section was by State Key Lab of Advanced Metals and Materials 2021-ZD08 and the fundamental research funds for the Central Universities (Grant No. 2020YJS145).

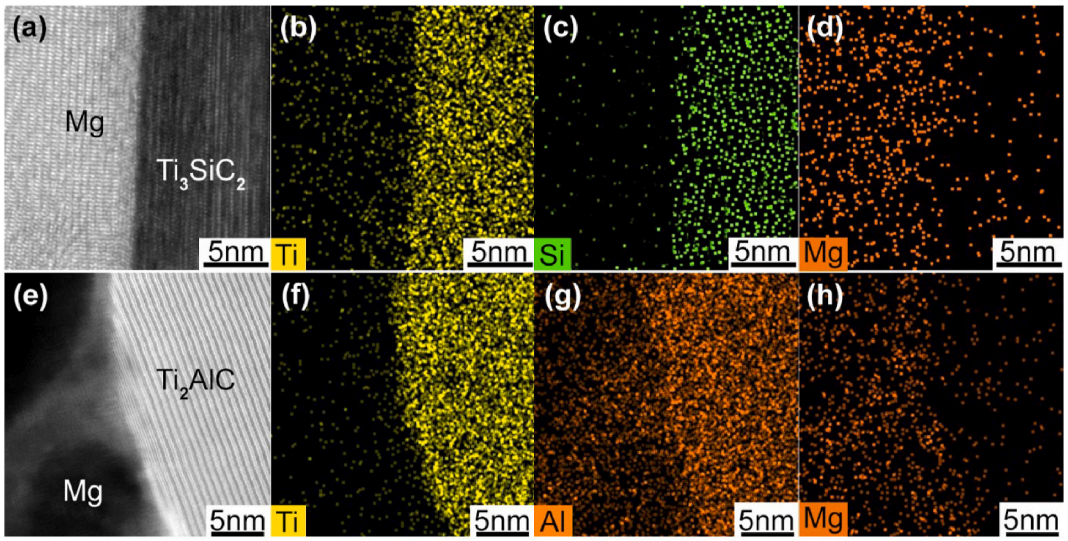

Fig. 8. HAADF-STEM images of the interfaces and the corresponding EDX maps of Ti_3SiC_2 (a–d) and Ti_2AlC (e–h) interfaces.

Acknowledgement

This work was supported by the National Natural Science Foundation of China (No. 52175284 and 51701010), the State Key Lab of Advanced Metals and Materials (No. 2021-ZD08), the Fundamental Research Funds for the Central Universities (No. 2020YJS145) and the Beijing Government Funds for the Constructive Project of Central Universities (No. 353139535).

References

[1] W.J. Joost, P.E. Krajewski, Scripta Mater. 128 (2017) 107–112.
[2] L. Tian, A. Russell, T. Riedemann, S. Mueller, I. Anderson, Mater. Sci. Eng., A 690 (2017) 348–354.
[3] M.P. Staiger, A.M. Pietak, J. Huadmai, G. Dias, Biomaterials 27 (2006) 1728–1734.
[4] B. Song, N. Guo, T. Liu, Q. Yang, Mater. Des. 62 (2014) 352–360, 1980-2015.
[5] W.J. Joost, JOM (J. Occup. Med.) 64 (2012) 1032–1038.
[6] X.J. Wang, D.K. Xu, R.Z. Wu, X.B. Chen, Q.M. Peng, L. Jin, Y.C. Xin, Z.Q. Zhang, Y. Liu, X.H. Chen, G. Chen, K.K. Deng, H.Y. Wang, J. Mater. Sci. Technol. 34 (2018) 245–247.
[7] T.T.T. Trang, J.H. Zhang, J.H. Kim, A. Zargaran, J.H. Hwang, B.C. Suh, N.J. Kim, Nat. Commun. 9 (2018) 2522.
[8] M. Barsoum, T. Zhen, S. Kalidindi, M. Radovic, A. Murugaiah, Nat. Mater. 2 (2003) 107–111.
[9] W. Yu, V. Mauchamp, T. Cabioc'h, D. Magne, L. Gence, L. Piraux, V. Gauthier-Brunet, S. Dubois, Acta Mater. 80 (2014) 421–434.
[10] Z. Sun, Int. Mater. Rev. 56 (2011) 143–166.
[11] X. Pi, W. Yu, C. Ma, X. Wang, S.M. Xiong, A. Guitton, Materials 13 (2020).
[12] B. Anasori, E.A.N. Caspi, M.W. Barsoum, Mater. Sci. Eng., A 618 (2014) 511–522.
[13] F. Labib, H.M. Ghasemi, R. Mahmudi, Wear 348–349 (2016) 69–79.
[14] I. Aatthisugan, A. Razal Rose, D. Selwyn Jebadurai, Journal of Magnesium and Alloys 5 (2017) 20–25.
[15] A. Das, S.P. Harimkar, J. Mater. Sci. Technol. 30 (2014) 1059–1070.
[16] B. Anasori, S. Amini, V. Presser, M.W. Barsoum, Nanocrystalline Mg-matrix composites with ultrahigh damping properties, in: W.H. Sillekens, S.R. Agnew, N. R. Neelameggham, S.N. Mathaudhu (Eds.), Magnesium Technology 2011, Springer International Publishing, Cham, 2016, pp. 463–468.
[17] W. Yu, D. Chen, L. Tian, H. Zhao, X. Wang, J. Mater. Sci. Technol. 35 (2019) 275–284.
[18] W. Yu, H. Zhao, X. Wang, L. Wang, S. Xiong, Z. Huang, S. Li, Y. Zhou, H. Zhai, J. Alloys Compd. 730 (2018) 191–195.
[19] W. Yu, X. Li, M. Vallet, L. Tian, Mech. Mater. 129 (2019) 246–253.
[20] W. Yu, H. Zhao, X. Hu, J. Alloys Compd. 732 (2018) 894–901.
[21] J. Wang, Y. Zhou, T. Liao, J. Zhang, Z. Lin, Scripta Mater. 58 (2008) 227–230.
[22] H. Wang, H. Han, G. Yin, C.-Y. Wang, Y.-Y. Hou, J. Tang, J.-X. Dai, C.-L. Ren, W. Zhang, P. Huai, Materials 10 (2017) 103.
[23] S. Amini, J.M. Córdoba Gallego, L. Daemen, A.R. McGhie, C. Ni, L. Hultman, M. Oden, M.W. Barsoum, Nano Lett. 9 (2009) 3082–3086.
[24] W.B. Yu, X.J. Wang, H.B. Zhao, C. Ding, Z.Y. Huang, H.X. Zhai, Z.P. Guo, S. M. Xiong, J. Alloys Compd. 702 (2017) 199–208.
[25] J. Hashim, L. Looney, M. Hashmi, J. Mater. Process. Technol. 92 (1999) 1–7.
[26] J. Hashim, L. Looney, M. Hashmi, J. Mater. Process. Technol. 123 (2002) 251–257.
[27] M.W. Barsoum, T. El-Raghy, Metall. Mater. Trans. (2000) 31A.
[28] M. Radovic, M.W. Barsoum, A. Ganguly, T. Zhen, P. Finkel, S.R. Kalidindi, E. Lara-Curzio, Acta Mater. 54 (2006) 2757–2767.
[29] B. Anasori, N.C. El'ad, M.W. Barsoum, Mater. Sci. Eng., A 618 (2014) 511–522.
[30] S. Amini, C. Ni, M.W. Barsoum, Compos. Sci. Technol. 69 (2009) 414–420.
[31] A. Sanaty-Zadeh, Mater. Sci. Eng., A 531 (2012) 112–118.
[32] L. Tian, L. Li, International Journal of Current Engineering and Technology 8 (2018) 236–249.
[33] S. Khoddam, L. Tian, T. Sapanathan, D. Hodgson Peter, A. Zarei-Hanzaki, Adv. Eng. Mater. (2018), 0.
[34] X. Xu, T.L. Ngai, Y. Li, Ceram. Int. 41 (2015) 7626–7631.